International Journal of Applied Earth Observation and Geoinformation 135 (2024) 104250

Contents lists available at ScienceDirect

International Journal of Applied Earth Observation and Geoinformation

journal homepage: www.elsevier.com/locate/jag

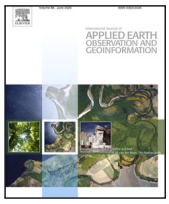

Multispectral imaging and terrestrial laser scanning for the detection of drought-induced paraheliotropic leaf movement in soybean

Erekle Chakhvashvili [a,*], Lina Stausberg [b], Juliane Bendig [a], Lasse Klingbeil [b], Bastian Siegmann [a], Onno Muller [a], Heiner Kuhlmann [b], Uwe Rascher [a]

[a] Forschungszentrum Jülich - IBG2, Wilhelm-Johnen Strasse, Jülich, 52428, NRW, Germany
[b] Institute of Geodesy and Geoinformation (IGG), University of Bonn, Nussallee 17, Bonn, 53115, NRW, Germany

ARTICLE INFO

Keywords:
Leaf inclination angle
PROSAIL
UAV
TLS
Paraheliotropism

ABSTRACT

Plant foliage is known to respond rapidly to environmental stressors by adjusting leaf orientation at different timescales. One of the most fascinating mechanisms is paraheliotropism, also known as light avoidance through leaf movement. The leaf orientation (zenith and azimuth angles) is a parameter often overlooked in the plant and remote sensing community due to its challenging measurement procedures under field conditions. In this study, we investigate the synergistic potential of uncrewed aerial vehicle (UAV)-based mutlispectral imaging, terrestrial laser scanning (TLS) and radiative transfer model (RTM) inversion to identify the paraheliotropic response of two distinct soybean varieties: Minngold, a chlorophyll-deficient mutant, and Eiko, a wild variety. We examined their responses to drought stress during the boreal summer drought in 2022 in western Germany by measuring average leaf inclination angle (ALIA) and canopy reflectance. Measurements were taken in the morning and at midday to track leaf movement. Our observations show significant differences between the paraheliotropic response of both varieties. Eiko's terminal and lateral leaves became vertically erect in the midday (54 → 61°), while Minngold's ALIA remained largely unchanged (52 → 57°). Apart from the vertical leaf movement, we also observed leaf inversion (exposing the abaxial side of the leaf) in Eiko under extreme water scarcity. The red edge band at 740 nm showed the strongest correlation with ALIA (r^2 = 0.52 – 0.76) The ratio of the far red edge to near infrared (RE740/NIR842) vegetation index compensated for varying light levels during morning and afternoon measurements, exhibiting strong correlations with ALIA when considering only sun-lit leaf spectra (r^2 = 0.72). The retrieval of ALIA with PROSAIL varied based on ALIA constraints and the spectra used for retrieval (full spectrum or the combination of bands 742 and 842), resulting in a root mean square error (RMSE) of 7.7-12.9°. PROSAIL faced challenges in simulating the spectra of plots with very low LAI due to the soil background. This study made the first attempt to observe different paraheliotropic responses of two soybean varieties with UAV-based multispectral imaging. Proximal sensing opens up the possibilities to observe early stress indicators such as paraheliotropism, at much higher spatial and temporal resolution than ever before.

1. Introduction

Monitoring crop biophysical parameters has gained increased importance due to the challenges arising from extreme climatic and biotic events (Intergovernmental Panel on Climate Change (IPCC), 2023). Water, heat and light stress are primary contributors to crop yield reduction (Fahad et al., 2017). Plants exhibit various adaptations to combat these stressors, including chloroplast movement (Haupt and Scheurlein, 1990), changes in chlorophyll concentration (Murchie and Horton, 1997), non-photochemichal quenching (NPQ) (Müller et al., 2001) and paraheliotropism also known as light-avoidance through leaf movement (Pastenes, 2004; Ludlow and Björkman, 1984). Paraheliotropism involves changes of turgor pressure at the base of lamina (Nilsen and Forseth, 2018), causing leaves to align parallel to the incident light. This way plants avoid high leaf temperature, high evapotranspiration (Ehleringer and Forseth, 1980; Forseth and Ehleringer, 1982), and photoinhibition during drought (Ludlow and Björkman, 1984).

* Corresponding author.
E-mail addresses: e.chakhvashvili@fz-juelich.de (E. Chakhvashvili), lina.zabawa@igg.uni-bonn.de (L. Stausberg), j.bendig@fz-juelich.de (J. Bendig), klingbeil@igg.uni-bonn.de (L. Klingbeil), b.siegmann@fz-juelich.de (B. Siegmann), o.muller@fz-juelich.de (O. Muller), heiner.kuhlmann@uni-bonn.de (H. Kuhlmann), u.rascher@fz-juelich.de (U. Rascher).

https://doi.org/10.1016/j.jag.2024.104250
Received 22 April 2024; Received in revised form 8 October 2024; Accepted 27 October 2024
Available online 15 November 2024

Paraheliotropism is commonly seen in legumes such as soybean (Meyer and Walker, 1981; Oosterhuis et al., 1985; Kao and Forseth, 1992). Owing to its significance as an essential source of protein for both humans and animals (Liu et al., 2020), monitoring the health status of soybean in the face of adverse environmental events, such as drought, is important. Drought is the condition of water scarcity caused by insufficient precipitation and/or increased evaporation, often resulting from higher-than-normal temperatures characteristic for the specific area (DWD, 2024). An early indicator of water scarcity in soybeans is the paraheliotropism (Meyer and Walker, 1981). Typical leaf movement patterns involve erecting leaves vertically during midday as well as leaf inversion (exposing the abaxial side) in the presence of extreme drought.

Leaf movement can be characterized by leaf orientation parameters, one of which is the average leaf inclination angle (ALIA). ALIA is described as an angle between leaf normal and the zenith. It influences light interception, photosynthesis efficiency, competition in plant canopies and acts as an early stress indicator (Yang et al., 2023). Despite its importance, ALIA has been relatively overlooked due to the challenges associated with in-situ measurements being laborious and error-prone. Many studies opt for indirect retrieval methods instead of in-situ ones, which include photographic (Zou et al., 2014; Müller-Linow et al., 2015) and laser scanning approaches, (Bailey and Mahaffee, 2017) allowing diurnal and almost instantaneous measurements of ALIA under field conditions. While these systems deliver good results, they face limitations in scalability due to their labor-intensive measurement procedures. The efficiency of these systems diminishes as the study area expands. The challenge arises from the rapid changes in leaf orientation parameters over time, making the measurement process more difficult for larger areas. An alternative, yet under-explored, approach to measure ALIA involves radiative transfer models (RTMs) using optical data acquired from airborne platforms. This method offers faster and easier data acquisition compared to traditional methods, holding significant potential for wider application.

Together with leaf area index (LAI), ALIA is an important parameter for radiation transfer within the canopy and significantly contributes to the signal detected by optical sensors. While a substantial research attention has been given to LAI as a proxy for physiological processes retrieval of ALIA using RTMs has been understudied (Berger et al., 2018). RTMs simulate absorption, transmittance and reflectance of single leaves or plant canopies. Due to their physical nature, RTMs can be universally applied, which eliminates the need to calibrate the model to specific sensor, crop or geographical location. The most widely used RTM, PROSAIL, which is a coupled leaf- (PROSPECT) (Jacquemoud and Baret, 1990) canopy (SAIL) (Verhoef, 1984) model, employs ALIA as one of the main structural input parameters. ALIA exhibits high sensitivity in the red edge and near-infrared (NIR) regions and shares this sensitivity with LAI (Jacquemoud et al., 2009; Zou et al., 2014). Given their similar impact on the reflectance spectrum, prior knowledge of ALIA should be incorporated as a constraint (Jacquemoud, 1993), highlighting the importance of field-based ALIA measurements.

RTMs have primarily been applied to satellite data, which often lacks the necessary spatial and temporal resolution to be effective in high-throughput field phenotyping applications. In contrast, uncrewed aerial vehicles (UAVs) deliver both the required spatial and temporal resolution.

Rapid developments in UAV technology opened up ways for retrieving crop parameters at centimeter-level spatial scales (Berni et al., 2009; Yang et al., 2017). UAVs are versatile in terms of sensor payloads and flight parameters (altitude, direction, etc.) which in turn enables exploring parameter retrieval using various flight configurations. Additionally, UAV images allow to discriminate between different canopy constituents (soil, shaded leaves, sun-lit leaves) and study them separately. UAVs have been used to retrieve crop parameters using parametric (Berni et al., 2009; Kanning et al., 2018), machine learning (Du et al., 2022) and physical models (Verger et al., 2014; Chakhvashvili et al., 2022). While there is a considerable research on the retrieval of LAI from UAV-based multispectral or hyperspectral imaging, only a few studies have explored ALIA retrieval (Zou and Mõttus, 2015), particularly in the context of paraheliotropic response of the plants.

This study aims to explore the paraheliotropic response of two soybean varieties by quantifying ALIA using terrestrial laser scanning, multispectral imaging, and RTM inversion. We employed TLS and high-resolution multispectral UAV imagery along with the PROSAIL RTM. Measurements were conducted at three time points during the vegetation period. Morning and afternoon measurements were taken on two occasions to track diurnal leaf movement. PROSAIL was parameterized with field-collected data, and ALIA was retrieved using a LUT-based inversion approach.

Table 1
Flight times during summer season of 2022. SZA - solar zenith angle; DAS - days after sowing.

Date	Time of the day	Flight time	SZA	DAS	Illumination conditions
June 14	Afternoon	12:37–12:56	29	42	Sunny
July 13	Morning	9:00–9:20	60	71	Sunny
	Afternoon	14:00–14:20	29		Sunny
August 10	Morning	8:30–8:40	70	98	Sunny
	Afternoon	13:05–13:15	35		Sunny

2. Materials and methods

2.1. Study area

The study area is situated at the agricultural research station Campus Klein-Altendorf, within the state of North Rhine-Westphalia, (latitude 50°37′N, longitude 6°59′E, elevation 176 m) in Germany. The annual average precipitation is 603 mm, while the average annual temperature over the long term is 9.4 °C. A soybean experiment, consisting of two varieties (Eiko and Minngold) was sown in two densities (30 and 60 seeds/m^2) in 1.5 × 3 m plots (Fig. 1). Minngold (University of Minnesota) is a chlorophyll-deficient mutant characterized by lower chlorophyll content in the upper leaves compared to the lower leaves (Campbell et al., 2015). Several studies have assessed the photosynthetic performance of this mutant (Sakowska et al., 2018; Genesio et al., 2020). Meanwhile, Eiko (Asgrow, USA) is a commercial soybean cultivar.

2.2. UAV data collection

Image data was acquired from a DJI Matrice PRO 600 UAV platform (SZ DJI Technology Co., Ltd., Schenzhen, China). A 10 channel Micasense multi-camera array system (AgEagle Sensor Systems Inc., Wichita, KS, USA), was mounted on a Ronin MX gimbal attached to the UAV. The images are captured synchronously for each band as separate files. Images were obtained at 20 m above ground level, resulting in a ground sampling distance (GSD) of 1.39 cm. The flight altitude was optimized to balance high spatial resolution with proper scene reconstruction. The UAV was flown at a velocity of 3 m/s, resulting in a front-lap of 80% and side-lap of 70%. For more details on flight and camera setup see Chakhvashvili et al. (2021). Afternoon flights were conducted between 12:00–13:00 h local time on days with stable illumination conditions. Morning flights were conducted at 8:00–9:00 h (Table 1). A set of nine near-lambertian panels (Mankiewicz Gebr. & Co. GmbH & Co. KG, Hamburg, Germany) with different reflectance factors, ranging from dark (2%) to bright (63%), was placed within the experiment on bare soil during each flight.

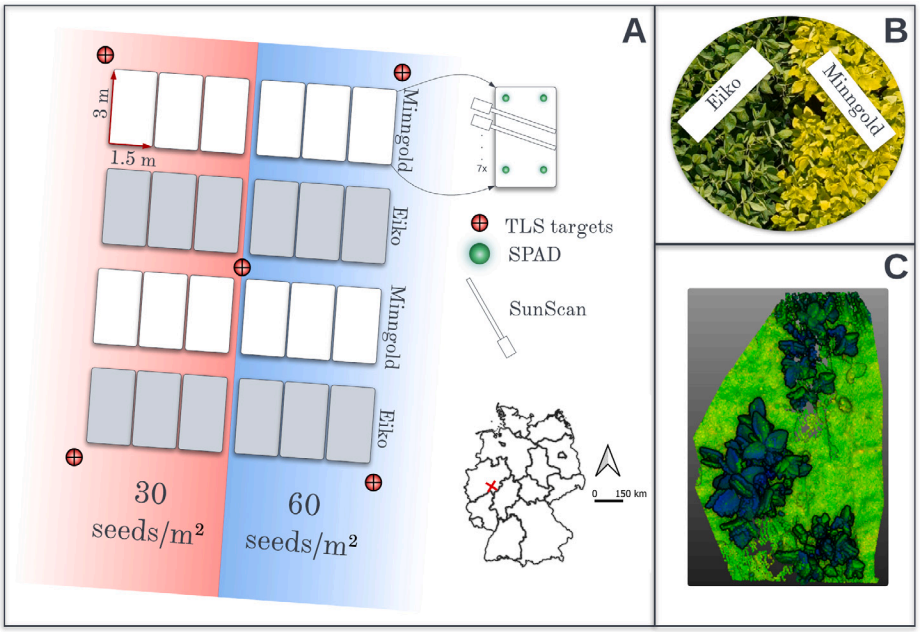

Fig. 1. Experimental design of soybean density experiment and measurement locations (A); RGB image of two soybean varieties taken from UAV (B); 3D point cloud of a soybean plot (C).

2.3. Image processing

Image data was processed in Agisoft Metashape Professional (Agisoft LLc, St. Petersburg, Russia). Images were stitched and georeferenced using ground control points that were evenly distributed in the field. At sensor radiance orthomosaics were generated by applying the Micasense radiometric calibration model using a python script within Metashape and exported for reflectance calibration as described in Chakhvashvili et al. (2021). To remove soil pixels from the UAV orthomosaics, we calculated the Excess Green (ExG) index (Woebbecke et al., 1995) and used adaptive manual thresholding to separate soil from plant pixels (range of 0.01–0.03). A manual threshold (range of 0.015–0.025) was used on the blue band to remove shaded pixels and to account for different lighting conditions.

2.4. Reference measurements

For the parametrization of the PROSAIL model, LAI and SPAD measurements were taken directly before or after the overflights Appendix. LAI was sampled non-destructively using a SunScan canopy analysis system (Delta-T Devices, UK). Destructive samples of both varieties were taken in selected plots in 2021 and 2022 after the overflights to validate SunScan measurements. Four plants were randomly selected in each plot and leaf area was measured with a leaf area meter (LI-3100C Area Meter, LI-COR Biosciences, Lincoln, USA). Prior to derivation of LAI from destructive samples, the number of plants per plot was manually counted. For the non-destructive measurements, the SunScan rod was placed diagonally to the crop rows into the canopy seven times in each plot (see Fig. 1) and the result was averaged. Consolidated data from 2021 and 2022 can be seen in Fig. A.10. The largest uncertainties were found in plots with heterogeneous distribution of soybean plants. For SPAD measurements, two plants were randomly selected in each plot. Measurement procedure differed for Minngold and Eiko. For Eiko three upper leaves were measured, each leaf four times. For Minngold the three upper and three lower leaves were measured, each leaf four times to account for variability in chlorophyll content in Minngold canopy layers.

2.5. TLS measurements

Terrestrial laser scanning (TLS) measurements were taken prior to the UAV flights at two different times on the same day. For data acquisition, five Leica tilt-and-turn targets were positioned at the specific locations in the field (Fig. 1). Scans were performed with a Leica ScanStation P50 (Leica Geosystems, Heerbrugg, Switzerland) with a spatial resolution of 6.3 mm at 10 m distance to the scanner. In order to scan the entire field at a sufficiently high resolution, the TLS was placed at 15 different positions in and around the field. These scans were spatially registered to each other by a target-based registration using the software *Leica Cyclone*. The result is a 3D point cloud, which contains x, y and z components. The whole measurement with the 15 positions took 3 h.

2.6. ALIA estimation

To estimate ALIA values from TLS measurements, a surface representation of the plants in each plot was reconstructed, using a fully automated pipeline implemented in Open3D (Zhou et al., 2018). A statistical approach was used that removes points that are farther away from their neighbors compared to the average point distance of the entire point cloud. In empirical experiments it was shown that five neighbors and a standard deviation of 1.0 are suitable parameters. To reduce the computation time, the point cloud is uniformly sub-sampled which reduced the point number P to P/k. The down-sampling parameter k was determined directly from the data set by choosing a point density of 40 points per $1\,cm^2$. The surface was reconstructed using the Ball-Pivoting algorithm (Bernardini et al., 1999), which creates a triangular mesh from the point cloud. A virtual ball with a radius ρ is placed onto the point cloud, with the radius determined based on the average point distance. This process is repeated three times with a scaling factor of 10 to ensure connectivity. Finally, any remaining holes in the mesh are detected, extracted, and filled with a flat surface, identified by being surrounded by boundary edges. To correct only the holes within the surface, the threshold value of the boundary edges e is set to $e \leq 30$. All holes with a lower number of boundary edges than e are filled with flat triangles, resulting in an almost completely closed surface model.

Table 2
PROSAIL variable ranges used in the construction of LUT.

Variable	Description	Range	Distribution
PROSPECT-5			
N	Leaf structure index	1.2–1.8	Uniform
C_{ab}/LCC [µg/cm^2]	Leaf chlorophyll content	0–70	Gaussian
C_{cx} [µg/cm^2]	Leaf carotenoid content	–	–
C_{bp} [unitless]	Brown pigments	0–0.5	Fixed/Uniform
C_m [g/cm^2]	Dry matter content	0.004–0.0075	Uniform
C_w [g/cm^2]	Leaf water content	–	–
4SAIL			
LAI [m^2/m^2]	Leaf area index	3	Fixed
ALIA [°]	Average leaf inclination angle	0–90/35–70	Step of 1
Hot	Hot spot parameter	0.01–0.5	Uniform
ρ_{soil} [%]	Soil reflectance	Extracted from image	–
SZA [°]	Sun zenith angle	Different for each date	–
OZA [°]	Observer zenith angle	0	–
rAA [°]	Relative azimuth angle	0	–

After generating the meshed surface of joined triangles, this representation was used to calculate the $ALIA$ values for each experimental plot. First the normal vectors $\vec{n} = (n_x, n_y, n_z)$ of the triangles were calculated and aligned in one direction. Afterwards, the different components of the normal vectors were used to determine the distribution of the leaf inclination angles θ using $\theta = \arccos(n_z)$. The median value of the resulting distribution than is calculated to get the $ALIA$ value as $ALIA = \overline{\theta}$.

2.7. Environmental data collection

Environmental data (precipitation, temperature and soil water content) were collected at the study site. A weather station (Wilmers Messtechnik GmbH, Hamburg, Germany) was located 200 m away from the experiment recorded temperature, precipitation and other parameters every 10 min. SoilNet (Bogena et al., 2010) sensors that measure soil water content (SWC) were installed within the same field at three different depths (10, 20 and 50 cm). The sensor was logging SWC at 15 min intervals.

2.8. PROSAIL parametrization and inversion

PROSAIL parametrization was done partly based on the reference measurements (Table 2) and partly using the parameter ranges available in the literature (Berger et al., 2018). The leaf optical depth (N-parameter) was calculated using PROSPECT-PRO (Féret et al., 2021) and the leaf optical measurements (leaf reflectance and transmittance measured with a field spectrometer) acquired during the SoyFlex campaign in 2016 (SoyFlex 2016). N-parameter was sampled using uniform distribution. A range of leaf chlorophyll content (LCC) with Gaussian distribution (mean 30 [µg/cm^2], standard deviation 5) was used to construct the look-up table (LUT). LAI was fixed to avoid confounding effects on ALIA. Two ALIA scenarios were simulated: (a) no constrain of ALIA, (b) ALIA constrained to the values that were observed (± 5 added to upper and lower limits) in the field. Soil reflectance was extracted from the bare soil areas in the multispectral orthomosaics. Solar zenith angles were calculated for each date and time. A global sensitivity analysis was performed to confirm the sensitivity of ALIA and LAI in the red edge and NIR bands of the multispectral sensor.

The Look-Up-Table (LUT) inversion scheme was used to retrieve ALIA. For this purpose, 10.000 simulations were selected out of every possible combination, using latin hypercube sampling. The full spectrum was used for the model inversion with 2% of Gaussian noise added to the spectra. To find the best match between simulated and measured reflectance we used simple RMSE (root-mean square error) as a cost function.

3. Results

3.1. Hydrometeorological conditions at the study site

The Fig. 2 displays environmental data, including weekly temperature and precipitation measurements, as well as continuous SWC measurements at three different depths. The summer of 2022 exhibited exceptionally dry conditions, as evident from the climate diagram. There was little to no precipitation in the months of June (26.9 mm), July (4.2 mm) and August (0.6 mm). For reference, the long term average precipitation (1961–1990) recorded at DWD station (Deutscher Wetterdienst), located 30 km northeast from the study site at Cologne-Bonn Airport for the months June, July and August are 86, 84 and 77 mm, respectively (Deutscher Wetterdienst, 2023). The mean daily temperatures during June, July, and August (18 °C, 19 °C, and 20 °C, respectively) exceed the corresponding long-term averages of 16 °C, 18 °C, and 18 °C (Deutscher Wetterdienst, 2023). Due to an extended period of drought, the soil water content (SWC) in the soil profile, extending to a depth of 50 cm, remained exceptionally low throughout the entire summer. Specifically, in the 10 cm layer, the SWC percentages were 12%, 12%, and 10% for the months of June, July, and August, respectively. In the 20 cm layer, the corresponding values were 16%, 14%, and 14%, while in the 50 cm layer, they were 22%, 19%, and 19%.

3.2. ALIA measurement results

The results of TLS measurements can be found in Fig. 3 represented as distribution plots with median values marked with vertical lines. Minngold and Eiko exhibited different diurnal patterns of leaf movement during every measurement. On the 14th of June a strong difference between ALIA of Minngold (51°) and Eiko (60°) was observed in the afternoon. The plants were still very small (BBCH stages (Biologische Bundesanstalt, Bundessortenamt und CHemische Industrie) 22–26) as can be seen on the RGB images.

On the 13th of July both varieties show similar ALIAs in the morning: 52°- Minngold and 54° Eiko. This trend changed in the afternoon measurement: Eiko's ALIA increased to 61°, while Minngold's remained stable at 54°. On the 10th of August, ALIA values of Eiko were higher (57°) compared to previous measurements, but increased further towards the afternoon (63°). In comparison, Minngold's leaf angle increased only slightly.

3.3. Relationship between ALIA and spectral bands

The results of global sensitivity analysis (Fig. 4) confirm the impact of ALIA on red edge and NIR regions (740–842 nm, light blue). ALIA

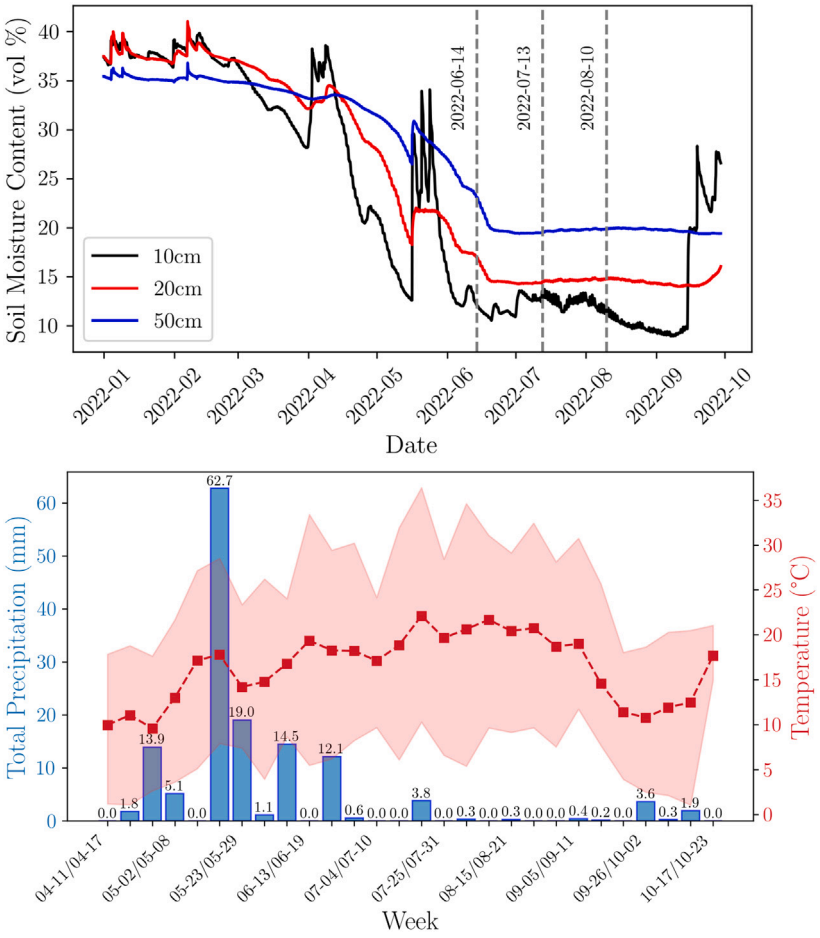

Fig. 2. Soil water content (upper plot) during January–October timespan and climate diagram (April–October) of the CKA study site in 2022.

shares this sensitivity with LAI (purple). Simulated reflectance of two spectral bands (742 and 842 nm) with changing sun zenith angle (morning and afternoon) displays that the canopy reflectance is not affected by the SZA.

To illustrate the relationship between ALIA and the visible/near-infrared bands of the multispectral camera, reflectance of each spectral band with soil and shaded pixels removed was compared to the median morning and afternoon TLS-derived ALIA measurements for both varieties (see Fig. 5). Morning measurements showed no correlation in the spectral bands that are expected to be sensitive to ALIA, specifically at 740 nm (r^2 = 0) and 842 nm (r^2 = 0.2). Minngold exhibits a generally higher correlation in the green (531 and 560 nm), red (650 and 668 nm) and red edge bands (705 and 717 nm) compared to Eiko.

The afternoon measurements show strong correlation in visible and red edge bands. For Minngold, the r^2 values range from 0.51 to 0.88, while for Eiko, they are between 0.47 and 0.74. Correlations are still higher for Minngold than Eiko. Compared to morning measurements correlations are much higher for both varieties, especially at 560 nm. Correlations are low for the bands located at 740 and 842 nm. For Minngold r^2 are 0 and 0.36, and for Eiko r^2 0.35 and 0.16 calculated for the bands at 740 and 842 nm, respectively.

To see the effect of plots with low LAI on the relationship with bands 740 and 842 nm, the June measurement was removed (Fig. 6). The correlation between band 740 (r^2 = 0.5 – 0.7) and ALIA improved significantly for the afternoon when removing June measurement, but did not change for the morning measurement and band 842. In order to differentiate the effects of LAI on spectral signature compared to ALIA, LAI was plotted against 740 and 842 nm bands. We observed higher correlations between LAI and the two bands (r^2 = 0.4 – 0.7) in the morning compared to ALIA and no correlation in the afternoon.

Since the anticipated correlations of ALIA with the reflectance data at 740 nm and 842 nm were not observed, we explored the ratio of the two bands. The results are depicted in Fig. 7. We examined the relationships using different image processing approaches: (a) averaging spectra per plot using every pixel (soil, plants, and shade), (b) averaging spectra without soil pixels (but including shade), and (c) averaging spectra without soil and shade (pure plant pixels). The highest correlation was found for approach (c) using pure plant pixels, with an r^2 value of 0.72. The relation between LAI and the RE/NIR ratio was also tested to rule out the influence of LAI on the ALIA RE/NIR ratio relationship. The lower row in Fig. 7 shows the low correlations (r^2 = 3.55 – 0.44) determined for the three approaches.

3.4. ALIA retrieved using PROSAIL

The results of ALIA retrieved with PROSAIL using the full spectrum are depicted in Fig. 8. In Panel (b) and (d) in Fig. 8 the measurements recorded on the first data acquisition day (16 June) were removed from the analysis as uncertainties associated with PROSAIL simulations of very low LAI canopies was high. ALIA for the non-constrained case are significantly underestimated (Fig. 8 a, b; RMSE 13°), compared to the constrained case (Fig. 8 c, d; RMSE 7.7 and 3.8 degrees, respectively). ALIA estimation based on PROSAIL worked significantly better for Minngold than Eiko. The PROSAIL simulation for Eiko having high ALIA does not match well the ALIA reference measurements.

Results depicting only selected bands (740 and 842 nm) and June measurements removed without constraining the model is displayed on Fig. 9. Compared to the full spectrum method the RMSE here is lower (6.68°), but r^2 is higher (0.64). There is a significant underestimation of the Minngold July measurement.

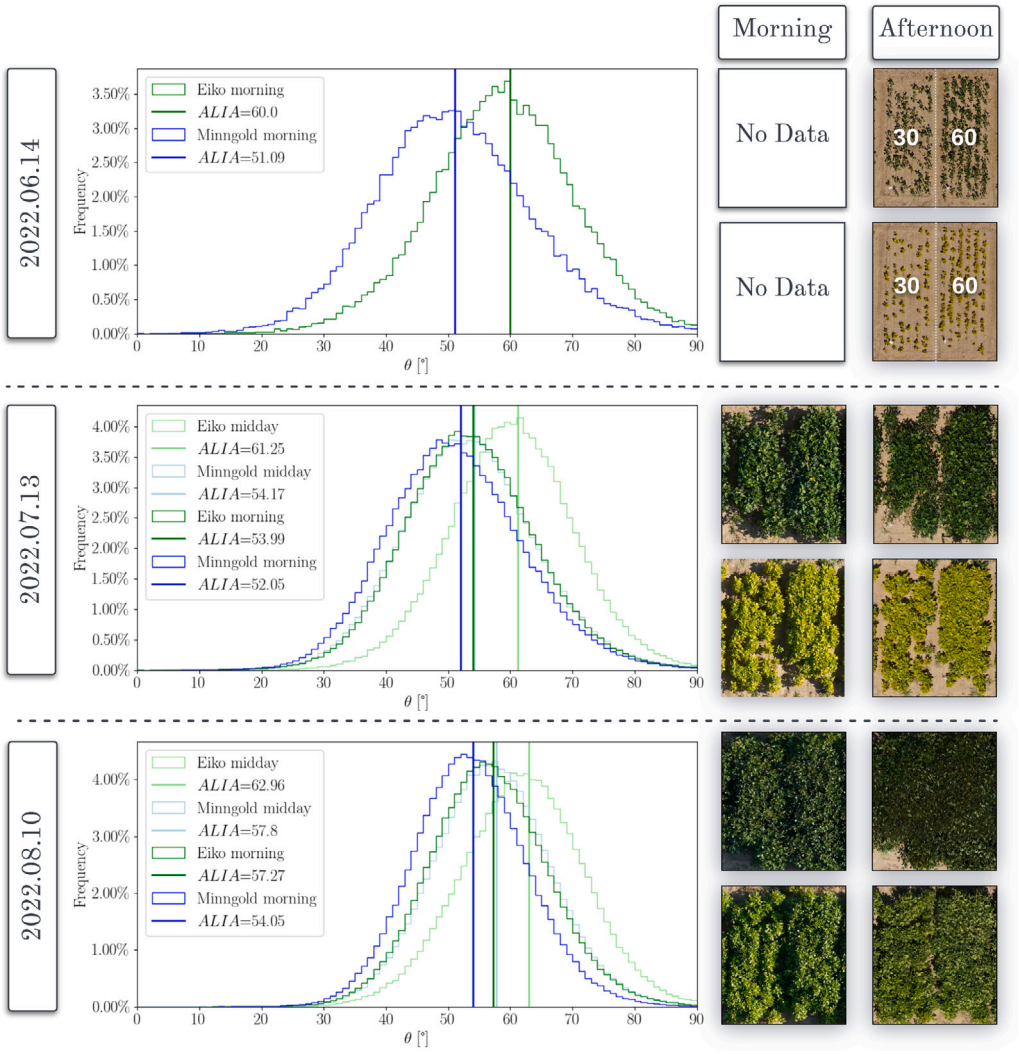

Fig. 3. (L) ALIA distributions of Minngold and Eiko varieties derived from TLS measurements acquired on 15th June, 13th July and 10th August in the morning and afternoon; (R) Example RGB images of soybean plots recorded during the morning and afternoon overflights at the respective days. The left subplots within each image had 30 kernels per square meter, the right subplot - 60.

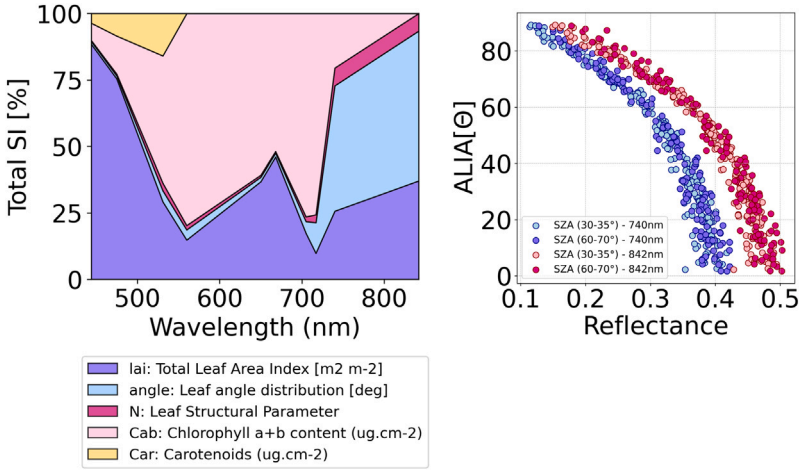

Fig. 4. Left plot: Results of the global sensitivity analysis (GSA) applied to reflectance spectra simulated with PROSAIL having the spectral resolution of the MicaSense Dual camera system. SI stands for Sobol Index. The sobol index helps to identify the importance of input variables, in this case crop parameters, on the model output. Right plot: PROSAIL simulated reflectance representative for morning (SZA 60–70°) and afternoon data acquisitions (SZA 30–35°) of the MicaSense dual red-edge (740 nm) and NIR (842 nm) spectral bands. SZA: sun zenith angle. (For interpretation of the references to color in this figure legend, the reader is referred to the web version of this article.)

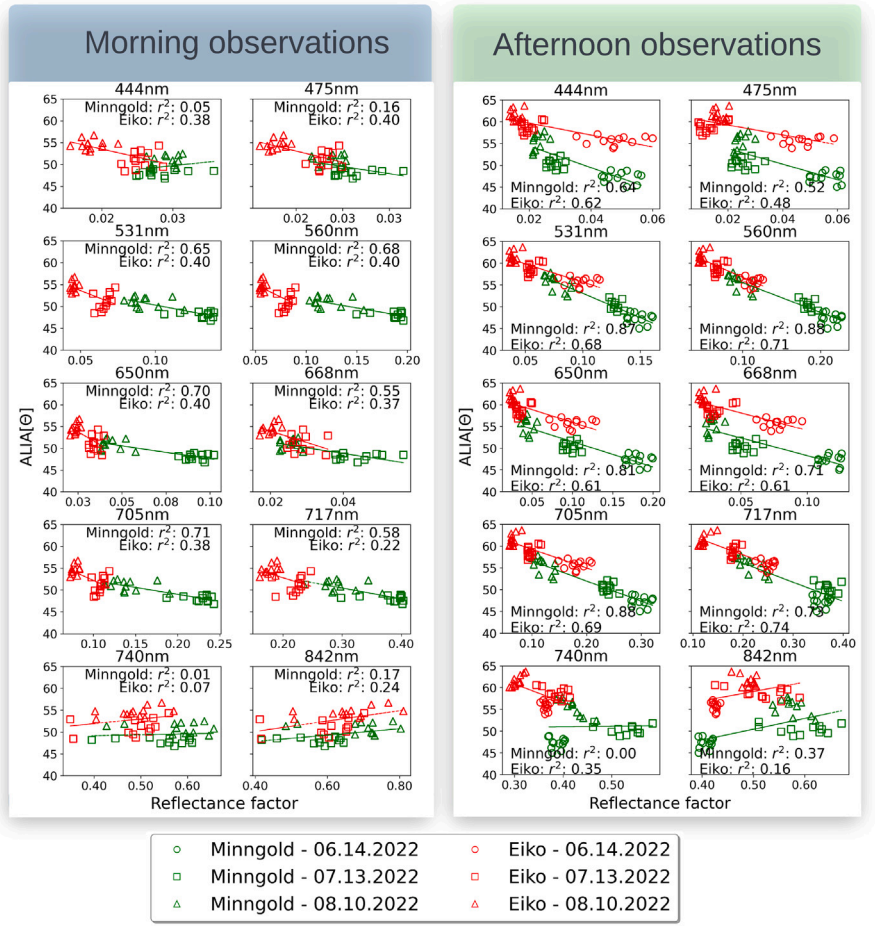

Fig. 5. Relationship between LIDAR-based ALIA and spectral bands from the UAV image data of Eiko and Minngold recorded during the morning and afternoon data acquisitions. (For interpretation of the references to color in this figure legend, the reader is referred to the web version of this article.)

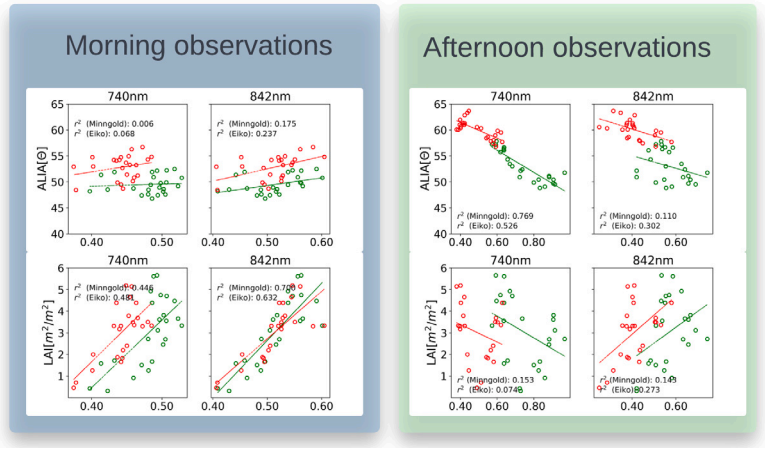

Fig. 6. (l) Correlations between ALIA, LAI and bands 740 and 842 nm with the June measurements removed during the morning; (r) correlations between ALIA, LAI and bands 740 and 842 nm during the afternoon with June measurements removed. The legend for color coding can be found in Fig. 5. (For interpretation of the references to color in this figure legend, the reader is referred to the web version of this article.)

4. Discussion

4.1. Paraheliotropic response of soybean varieties

Environmental variables collected at the study site strongly indicate drought during the boreal summer (Fig. 2). The area experienced an abnormal summer precipitation deficit of 215 mm and high temperature anomalies (>1.5 °C). Data from the German Drought Monitor (Zink et al., 2016) also confirm extreme drought throughout most parts of Germany by the end of August (reference period 1951–2015).

Leguminous plants are known to exhibit paraheliotropism when exposed to water scarcity and high temperatures (Meyer and Walker, 1981; Kao and Forseth, 1992). Diurnal TLS measurements revealed a notable discrepancy in the paraheliotropic response between Eiko

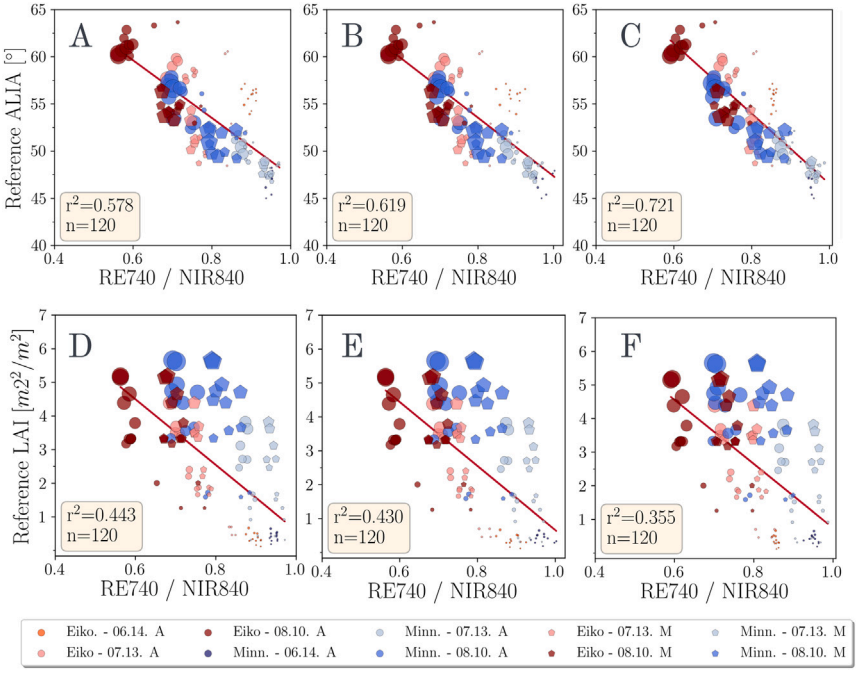

Fig. 7. Scatter plots showing the relationship of ALIA (A–C) and LAI with the Red Edge (740 nm) - near infrared (840 nm) ratio (D–F) using the three different image processing approaches. (A and D) soil and shaded pixels included in the image data (B and E) soil pixel removed but shaded pixels included in the image data; (C and F) soil and shaded pixels removed from the image data. (For interpretation of the references to color in this figure legend, the reader is referred to the web version of this article.)

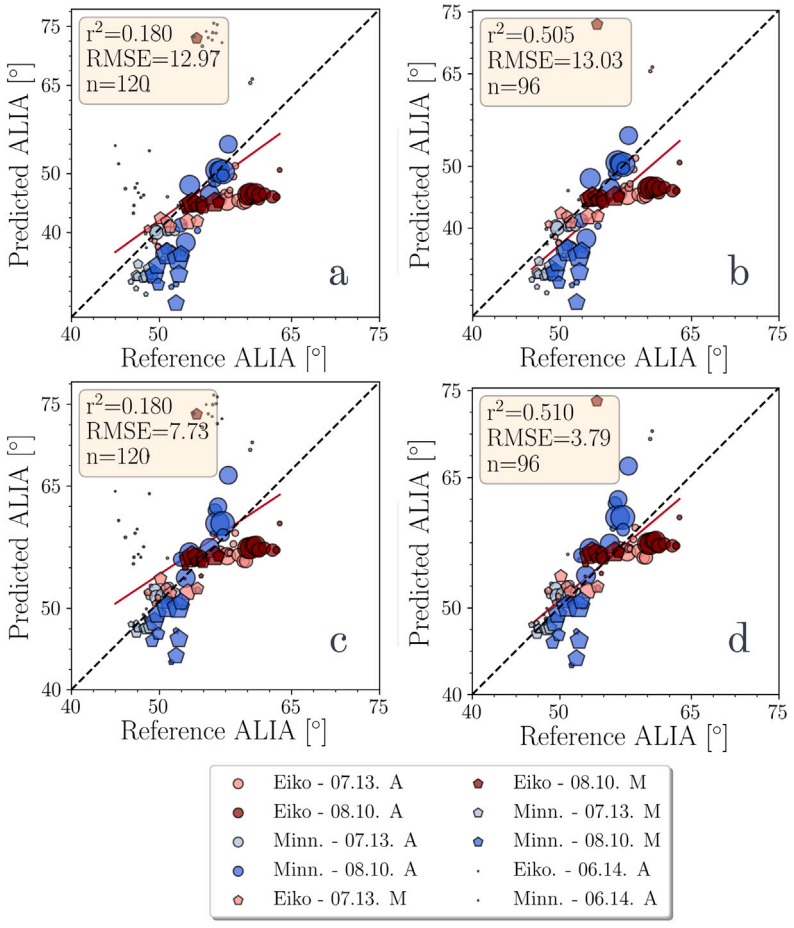

Fig. 8. Retrieval of ALIA using different approaches: (a) ALIA not constrained, data from 06.14 included; (b) ALIA constrained and 06.14 measurements removed; (c) ALIA's lower limit constrained and 06.14 data included; (d) ALIA's lower limit constrained and 06.14 data removed. Only the sunlit spectra were used for validation. Retrieval is based on the full spectrum; A stand for afternoon and M for morning measurements.

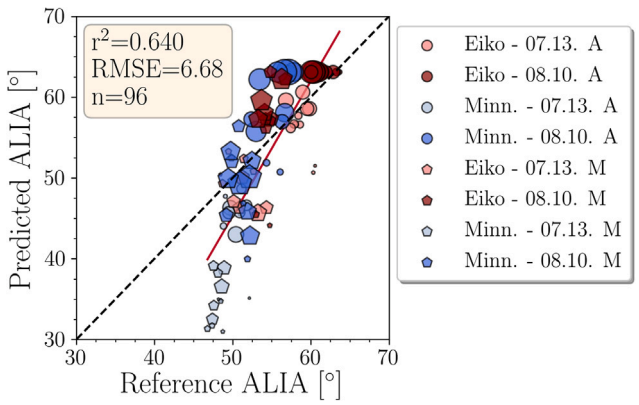

Fig. 9. ALIA retrieved using only bands 740 and 842 nm without constraining ALIA to the observed values.

and Minngold. In the mornings (8:00–9:00 AM local time), their leaf angles were similar (Fig. 3). However, in the afternoon, Eiko's leaves became vertical, while Minngold's remained largely unchanged. This response in Eiko is a classical example of paraheliotropism, documented in prior studies (Meyer and Walker, 1981; Oosterhuis et al., 1985; Kao and Forseth, 1992), but has not been tracked before using remote sensing methods. As the drought persisted throughout the entire boreal summer, we observed the gradual impact of water scarcity on Eiko. Our measurements revealed that the paraheliotropic response in June and July was characterized by terminal and lateral leaves becoming vertical in the afternoon. By August, when SWC was at its lowest, Eiko's leaves were already vertical in the morning. In the afternoon, we observed the inversion of the leaves, exposing the abaxial side (see images in Appendix). This phenomenon has been documented and various explanations have been proposed by Kao and Forseth (1992). The higher reflectance of the abaxial side, attributed to reflective trichomes, allows plants to reduce the thermo-radiative load, thereby lowering temperature and evapotranspiration rates and minimizing the inhibition of photosystem II.

In contrast to Eiko, Minngold exhibited a less pronounced paraheliotropic response. In fact, diurnal morning and afternoon measurements throughout the boreal summer showed minimal variation (range 51–58°). This subdued response in Minngold can be attributed to an additional defense mechanism against high light intensity and water scarcity. The genetic mutation causing the upper leaves to appear more yellow allows Minngold to reduce evapotranspiration rates by receiving a lower thermo-radiative load compared to the dark-leaved Eiko. Less chlorophyll content leads to decreased absorption of photosynthetically active radiation (APAR), thus more light is transmitted and reflected. Consequently, the paraheliotropic response in the upper leaves of Minngold is less evident. Previous studies have proposed that chlorophyll-deficient mutants, characterized by a higher surface albedo, could lead to significant water savings and help mitigate the effects of future heatwaves (Drewry et al., 2014; Sakowska et al., 2018), further highlighting the importance of breeding climate-resilient crop varieties.

Together with photosynthetic activity, variations in leaf temperature, and changes in the xanthophyll cycle, leaf movement serves as an important early stress indicator (Yang et al., 2023). Unlike leaf-level measurements of photosynthetic activity, which are often labor-intensive, possess limited spatial coverage, or lack sufficient resolution, tracking leaf movement using proximal multispectral imaging can be promising to be used in breeding applications to identify varieties better adapted to higher temperatures and lower water availability. This characteristic makes ALIA particularly compelling as one of the parameters to investigate early stress responses in various crops.

4.2. Effect of changing ALIA on the spectral reflectance of different soybean varieties

The red-edge and NIR part of the spectrum are most sensitive to changes in ALIA, as evident from the sensitivity analysis of the PROSAIL model (Jacquemoud, 1993)(Fig. 4). This sensitivity is shared with LAI, particularly in the NIR, creating challenges in disentangling the magnitude of the effects these two variables have on canopy reflectance. Zou et al. (2014) have demonstrated a negative correlation between canopy reflectance at 748 nm and ALIA across various crops, by using a hyperspectral image dataset acquired at a single time point.

In our results (Fig. 5), the interaction between ALIA and the single spectral bands differed with the time of the measurement. The high correlation coefficient observed for Minngold in both morning and afternoon, specifically in the visible range, can be attributed to variations in leaf chlorophyll content (LCC) throughout the summer. This variation was manifested by the increase of LCC of the upper and lower leaves in the canopy from July to August (Table A.3). In contrast, Eiko showed minimal changes in LCC during the same period. This leads us to infer that the correlation across most visible bands is driven by variations in LCC rather than by ALIA. This explanation does not hold true in the blue bands (444 and 475 nm), where a lower r^2 was observed for Minngold compared to Eiko. A possible reason for this discrepancy could be the significant reflectance of the blue light by the Minngold canopy, attributed to its transparent upper leaves and high light penetration rates, in contrast to Eiko.

Afternoon measurements reveal distinct trends in the correlation patterns between ALIA and single spectral bands. Both Eiko and Minngold exhibit high correlations in the visible range up to the red edge (740 nm) driven possibly by LCC variation rather than ALIA. Both varieties show lower correlations in the blue bands, albeit higher than those observed during the morning measurements. This discrepancy can be attributed to variations in photosynthetically active radiation (PAR) intensity between morning and afternoon, with the latter period providing higher PAR for plant canopies to redistribute energy. The varying correlations observed between 650 and 668 nm and ALIA for both varieties can be explained by differences in LCC between two varieties and light penetration, rather than disparities in ALIA.

At first glance in Fig. 5, the low r^2 at 740 nm and 842 nm in the afternoon appears inconsistent with the literature. However, these instances involve outliers, specifically plots with very low LAI values measured in June. When these extremely low LAI plots were removed from the analysis, the r^2 increased significantly for both varieties (Fig. 6). These results align with the findings of Zou et al. (2014), where the authors established a similar negative relationship between ALIA and the far red edge band (748 nm). The reflected light from the low LAI plots do not provide sufficient information on canopy architecture as reflectance is mostly from soil and only a small number of plant pixels are left after removing the soil background. The strong correlation does not extend to the NIR band, where a more substantial spread is observed. However, when combining data from both varieties, a general negative trend becomes apparent (Fig. 6).

Since no similar trend in relationship was found in the morning and afternoon between ALIA and the spectral bands at 740 nm and 842 nm, respectively, in comparison to the visible bands, it is suggested that the relationship is influenced by environmental factors, in this case difference in light intensity. Vegetation indices, compared to individual spectral bands, exhibit more pronounced sensitivity to vegetation parameters. This is due to the normalization of spectral bands as part of a vegetation index, which enhances the data and removes environmental effects (Holben and Justice, 1981). These effects, including different sun-target-sensor geometries, have been demonstrated by multiple studies to be mitigated with the help of ratioing (Kriegler, 1969; Vincent, 1972). Since the main difference between morning and afternoon measurements was the difference in sun-target-sensor

geometry, using the RE and NIR bands ratio, which is sensitive to ALIA (Fig. 7), seemed reasonable.

Differences in paraheliotropic mechanisms are also evident in Fig. 7 (panel C). The afternoon measurement for Eiko on 08.10 (represented by dark red dots) shows the highest leaf angles measured and the RE/NIR ratio is significantly lower than for other measured time-points. A possible explanation for this is the leaf inversion observed in Eiko on that day. The abaxial sides of the leaves have a higher albedo, that reduced the RE/NIR ratio.

Using the RE-NIR band ratio also helped in identifying whether changes in canopy reflectance were driven by ALIA or LAI. Fig. 7 shows that variability of RE/NIR cannot be explained by variability in LAI. The RE/NIR ratio remains constant during one measurement (either morning or afternoon) while the LAI changes.

4.3. ALIA retrieval

A limited number of studies have explored the retrieval of ALIA using imaging spectroscopy data, making the comparison of results rather challenging. Zou et al. (2014) and Zhou et al. (2018) used a hyperspectral imaging sensor to retrieve ALIA of various crops (faba beans, narrow-leafed lupin, turnip rape, oat, barley and wheat) in combination with PROSAIL modeling. The authors used a single band (748 nm) to retrieve ALIA (range 18–62°) with a reasonable accuracy (root mean squared error = 11.4°).

In our study we used ten wide spectral bands across the visible-near infrared range to explore PROSAIL's capability in retrieving ALIA, while fixing the LAI to 3. One notable challenge was simulating reflectance of low LAI value plots, particularly in the June data, where plants were still relatively small and surrounded by large soil areas (Fig. 3). Our assumption here is that after soil removal, little vegetation spectra was left, resulting in noisy data during the early growth stage. After removing the June date (Fig. 8), the outliers that remained were mostly plots with extremely low LAI values from the remaining two days, validating our initial assumption. Since we found correlations of ALIA with the spectral bands at 740 and 842 nm, it is also reasonable to assume that these two bands are sufficient for ALIA retrieval (Fig. 9). In the future different PROSAIL simulation configurations and retrieval algorithms should be explored to optimize ALIA retrieval. For example, hybrid approaches that combine RTMs with machine learning, can provide estimation uncertainties and provide parameter importance.

There was a discrepancy between the retrieval of ALIA of both soybean varieties. Eiko's ALIA retrieved from August 10 data exhibits almost no variation in predictions between morning and afternoon. This observation can be explained by the leaf inversion that was recorded on that day. Since the percentage of inversed leaves were much higher in the afternoon measurement, it had significant impact on the spectral signature (high reflectance over the entire visible-near infrared spectrum) of the whole canopy. This in turn made it difficult to simulate reflectance using PROSAIL, as it does not account for leaf inversion and assumes uniform distribution of plant pigments.

5. Conclusion and future perspectives

With this study, we present a novel approach to observe the drought-induced paraheliotropic response of two distinct soybean varieties, using multispectral imaging and terrestrial laser scanning. We demonstrate that UAV-based imaging sensors can be used to track leaf movement, covering large areas and eliminating the need of time and labor-intensive TLS measurements. The extremely dry summer in the study area in 2022 unveiled differences in response mechanisms between the chlorophyll-deficient mutant Minngold and the wild variety Eiko. Eiko exhibited increased leaf angle and leaf inversion under extreme drought, while Minngold showed minimal paraheliotropic response due to its low chlorophyll content. In the face of future extreme drought events predicted by climate models, it becomes increasingly important to study the defense mechanisms of crop varieties for breeding purposes.

We found a strong relationship between reflectance in the red edge (740 nm) and near-infrared (842 nm) bands and ALIA, particularly in afternoon measurements. The ratioing of these bands helped to combat variation in illumination condition between morning and afternoon data, revealing a correlation with ALIA. Even though a simple parametric model using a ratio index was sufficient to retrieve ALIA, further research is needed if the same correlations are valid for other crops and sensors. In this regard, RTMs like PROSAIL offer a transferable solution to the retrieval problem and should not be underestimated.

ALIA retrieval using PROSAIL showed reasonable accuracy, but reliability decreased for plots with very low LAI values. Constraining ALIA to observed values improved prediction accuracy. Future studies should explore the impact of other parameters, such as leaf chlorophyll content, and consider hybrid methods to enhance retrieval accuracy and efficiency.

CRediT authorship contribution statement

Erekle Chakhvashvili: Writing – review & editing, Writing – original draft, Visualization, Methodology, Investigation, Formal analysis, Data curation, Conceptualization. **Lina Stausberg:** Writing – review & editing, Writing – original draft, Visualization, Methodology, Investigation, Formal analysis, Data curation, Conceptualization. **Juliane Bendig:** Writing – review & editing, Supervision, Methodology. **Lasse Klingbeil:** Writing – review & editing, Supervision, Methodology. **Bastian Siegmann:** Writing – review & editing, Methodology. **Onno Muller:** Writing – review & editing. **Heiner Kuhlmann:** Writing – review & editing, Supervision. **Uwe Rascher:** Writing – review & editing, Supervision, Resources, Project administration, Funding acquisition.

Declaration of competing interest

The authors declare that they have no known competing financial interests or personal relationships that could have appeared to influence the work reported in this paper.

Acknowledgments

The authors would like to thank Maria del Pilar Cendrero Mateo for their help providing spectroscopy data from SoyFLex campaign and Zbyněk Malenovský for the interpretation of PROSAIL simulations. We would also like to thank Hannah Becker for support in the ground measurements.

The study was partially funded by the Deutsche Forschungsgemeinschaft (DFG, German Research Foundation) under Germany's Excellence Strategy—EXC 2070–390732324. The study was partially funded by the Deutsche Forschungsgemeinschaft (DFG, German Research Foundation) - 491111487.

Appendix. Measurements

See Fig. A.10 and Table A.3.

Data availability

Data will be made available on request.

Table A.3
Statistics of leaf area index (LAI) and leaf chlorophyll content (LCC) field measurements collected for Eiko and Minngold soybean varieties at CKA throughout the growing season; n—number of plots; Stdev—standard deviation, CV—coefficient of variation. Separation in LCC Minngold values marks the measurements of upper (left) and lower (right) leaves.

Variable	Soybean variety	Stat	06.14	13.07	03.08
LCC [µg/m^2]	Eiko	n	12	8	12
		Min	44.1	42.3	43.6
		Max	50.8	49.9	52.1
		Mean	47.6	45.8	49.3
		Stdev	2.3	2.5	2.7
		CV	0.04	0.04	0.05
	Minngold	n	12	12	12
		Min	6.2 | 12.6	5.5 | 14.2	10.6 | 24.0
		Max	8.6 | 23.4	8.5 | 20.6	21.1 | 32.8
		Mean	7.7 | 17.2	7.7 | 16.2	14.1 | 28.2
		Stdev	0.8 | 3.3	0.9 | 2.1	3.2 | 2.8
		CV	0.10 | 0.19	0.11 | 0.12	0.23 | 0.09
LAI [m^2/m^2]	Eiko	n	12	12	12
		Min	0.5	1.5	2.1
		Max	1.6	3.7	5.0
		Mean	0.9	2.9	3.5
		Stdev	0.3	0.8	0.8
		CV	0.37	0.27	0.22
	Minngold	n	12	12	12
		Min	0.5	2.0	1.9
		Max	0.7	3.3	4.6
		Mean	0.5	2.5	3.5
		Stdev	0.1	0.5	0.9
		CV	0.18	0.21	0.24

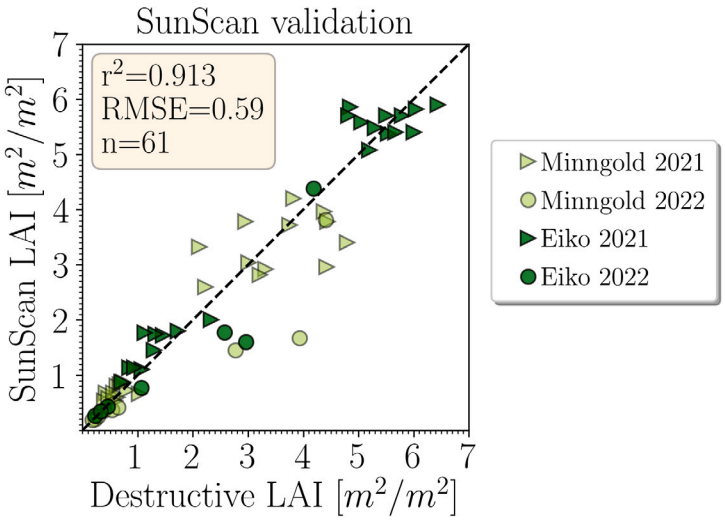

Fig. A.10. Validation of SunScan measurements with destructive samples. Destructive sampling was conducted in 2021 and 2022 for both soybean varieties.

References

Bailey, B.N., Mahaffee, W.F., 2017. Rapid measurement of the three-dimensional distribution of leaf orientation and the leaf angle probability density function using terrestrial LiDAR scanning. Remote Sens. Environ. 194, 63–76. http://dx.doi.org/10.1016/j.rse.2017.03.011.

Berger, K., Atzberger, C., Danner, M., D'Urso, G., Mauser, W., Vuolo, F., Hank, T., 2018. Evaluation of the PROSAIL model capabilities for future hyperspectral model environments: A review study. Remote Sens. 10 (1), 85. http://dx.doi.org/10.3390/rs10010085.

Bernardini, F., Mittleman, J., Rushmeier, H., Silva, C., Taubin, G., 1999. The ball-pivoting algorithm for surface reconstruction. IEEE Trans. Vis. Comput. Graphics 5 (4), 349–359. http://dx.doi.org/10.1109/2945.817351.

Berni, J.A., Zarco-Tejada, P.J., Suárez, L., Fereres, E., 2009. Thermal and narrowband multispectral remote sensing for vegetation monitoring from an unmanned aerial vehicle. IEEE Trans. Geosci. Remote Sens. 47 (3), 722–738. http://dx.doi.org/10.1109/TGRS.2008.2010457.

Bogena, H., Herbst, M., Huisman, J., Rosenbaum, U., Weuthen, A., Vereecken, H., 2010. Potential of wireless sensor networks for measuring soil water content variability. Vadose Zone J. 9 (4), 1002–1013. http://dx.doi.org/10.2136/vzj2009.0173.

Campbell, B.W., Mani, D., Curtin, S.J., Slattery, R.A., Michno, J.-M., Ort, D.R., Schaus, P.J., Palmer, R.G., Orf, J.H., Stupar, R.M., 2015. Identical substitutions in magnesium chelatase paralogs result in chlorophyll-deficient soybean mutants. G3: Genes Genomes Genet. 5 (1), 123–131. http://dx.doi.org/10.1534/g3.114.015255.

Chakhvashvili, E., Siegmann, B., Bendig, J., Rascher, U., 2021. Comparison of reflectance calibration workflows for a uav-mounted multi-camera array system. In: 2021 Int. Geosci. Remote Sens. Symp.. IGARSS, IEEE, pp. 8225–8228. http://dx.doi.org/10.1109/IGARSS47720.2021.9555143.

Chakhvashvili, E., Siegmann, B., Muller, O., Verrelst, J., Bendig, J., Kraska, T., Rascher, U., 2022. Retrieval of crop variables from proximal multispectral UAV image data using PROSAIL in maize canopy. Remote Sens. 14 (5), 1247. http://dx.doi.org/10.3390/rs14051247.

Deutscher Wetterdienst, 2023. Climate Diagram of Cologne/Bonn Airport. Deutscher Wetterdienst, URL: https://www.dwd.de/DWD/klima/beratung/ak/ak_105130_di.pdf. [Internet].

Drewry, D.T., Kumar, P., Long, S.P., 2014. Simultaneous improvement in productivity, water use, and albedo through crop structural modification. Global Change Biol. 20 (6), 1955–1967. http://dx.doi.org/10.1111/gcb.12567.

Du, L., Yang, H., Song, X., Wei, N., Yu, C., Wang, W., Zhao, Y., 2022. Estimating leaf area index of maize using UAV-based digital imagery and machine learning methods. Sci. Rep. 12 (1), 15937. http://dx.doi.org/10.1038/s41598-022-20299-0.

2024. Dwd. https://www.dwd.de/DE/service/lexikon/Functions/glossar.html?lv2=100578&lv3=603288. (Accessed 26 September 2024).
Ehleringer, J., Forseth, I., 1980. Solar tracking by plants. Science 210 (4474), 1094–1098. http://dx.doi.org/10.1126/science.210.4474.1094.
Fahad, S., Bajwa, A.A., Nazir, U., Anjum, S.A., Farooq, A., Zohaib, A., Sadia, S., Nasim, W., Adkins, S., Saud, S., et al., 2017. Crop production under drought and heat stress: plant responses and management options. Front. Plant Sci. 1147. http://dx.doi.org/10.3389/fpls.2017.01147.
Féret, J.-B., Berger, K., De Boissieu, F., Malenovskỳ, Z., 2021. PROSPECT-PRO for estimating content of nitrogen-containing leaf proteins and other carbon-based constituents. Remote Sens. Environ. 252, 112173. http://dx.doi.org/10.1016/j.rse.2020.112173.
Forseth, I.N., Ehleringer, J.R., 1982. Ecophysiology of two solar tracking desert winter annuals. Oecologia 54 (1), 41–49. http://dx.doi.org/10.1007/bf00541105.
Genesio, L., Bright, R.M., Alberti, G., Peressotti, A., Delle Vedove, G., Incerti, G., Toscano, P., Rinaldi, M., Muller, O., Miglietta, F., 2020. A chlorophyll-deficient, highly reflective soybean mutant: radiative forcing and yield gaps. Environ. Res. Lett. 15 (7), 074014. http://dx.doi.org/10.1088/1748-9326/ab865e.
Haupt, W., Scheurlein, R., 1990. Chloroplast movement. Plant Cell Environ. 13 (7), 595–614. http://dx.doi.org/10.1111/j.1365-3040.1990.tb01078.x.
Holben, B., Justice, C., 1981. An examination of spectral band ratioing to reduce the topographic effect on remotely sensed data. Int. J. Remote Sens. 2 (2), 115–133. http://dx.doi.org/10.1080/01431168108948349.
Intergovernmental Panel on Climate Change (IPCC), 2023. Weather and climate extreme events in a changing climate. pp. 1513–1766. http://dx.doi.org/10.1017/9781009157896.013.
Jacquemoud, S., 1993. Inversion of the PROSPECT+ SAIL canopy reflectance model from aviris equivalent spectra: theoretical study. Remote Sens. Environ. 44 (2–3), 281–292. http://dx.doi.org/10.1016/0034-4257(93)90022-P.
Jacquemoud, S., Baret, F., 1990. PROSPECT: A model of leaf optical properties spectra. Remote Sens. Environ. 34 (2), 75–91. http://dx.doi.org/10.1016/0034-4257(90)90100-Z.
Jacquemoud, S., Verhoef, W., Baret, F., Bacour, C., Zarco-Tejada, P.J., Asner, G.P., François, C., Ustin, S.L., 2009. PROSPECT+ SAIL models: A review of use for vegetation characterization. Remote Sens. Environ. 113, S56–S66. http://dx.doi.org/10.1016/j.rse.2008.01.026.
Kanning, M., Kühling, I., Trautz, D., Jarmer, T., 2018. High-resolution UAV-based hyperspectral imagery for LAI and chlorophyll estimations from wheat for yield prediction. Remote Sens. 10 (12), 2000. http://dx.doi.org/10.3390/rs10122000.
Kao, W.-Y., Forseth, I., 1992. Responses of gas exchange and phototropic leaf orientation in soybean to soil water availability, leaf water potential, air temperature, and photosynthetic photon flux. Environ. Exp. Bot. 32 (2), 153–161. http://dx.doi.org/10.1016/0098-8472(92)90040-9.
Kriegler, F., 1969. Preprocessing transformations and their effects on multspectral recognition. In: Proceedings of the Sixth International Symposium on Remote Sesning of Environment. pp. 97–131.
Liu, S., Zhang, M., Feng, F., Tian, Z., 2020. Toward a ‘‘green revolution’’ for soybean. Mol. Plant. 13 (5), 688–697. http://dx.doi.org/10.1016/j.molp.2020.03.002.
Ludlow, M.M., Björkman, O., 1984. Paraheliotropic leaf movement in Siratro as a protective mechanism against drought-induced damage to primary photosynthetic reactions: damage by excessive light and heat. Planta 161 (6), 505–518. http://dx.doi.org/10.1007/bf00407082.
Meyer, W.S., Walker, S., 1981. Leaflet orientation in water-stressed soybeans 1. Agron. J. 73 (6), 1071–1074. http://dx.doi.org/10.2134/agronj1981.00021962007300060039x.
Müller, P., Li, X.-P., Niyogi, K.K., 2001. Non-photochemical quenching. A response to excess light energy. Plant Physiol. 125 (4), 1558–1566. http://dx.doi.org/10.1104/pp.125.4.1558.
Müller-Linow, M., Pinto-Espinosa, F., Scharr, H., Rascher, U., 2015. The leaf angle distribution of natural plant populations: assessing the canopy with a novel software tool. Plant Methods 11, 1–16. http://dx.doi.org/10.1186/s13007-015-0052-z.
Murchie, E.H., Horton, P., 1997. Acclimation of photosynthesis to irradiance and spectral quality in British plant species: chlorophyll content, photosynthetic capacity and habitat preference. Plant Cell Environ. 20 (4), 438–448. http://dx.doi.org/10.1046/j.1365-3040.1997.d01-95.x.
Nilsen, E.T., Forseth, I.N., 2018. The role of leaf movements for optimizing photosynthesis in relation to environmental variation. In: The Leaf: A Platform for Performing Photosynthesis. Springer, pp. 401–423. http://dx.doi.org/10.1007/978-3-319-93594-2.
Oosterhuis, D.M., Walker, S., Eastham, J., 1985. Soybean leaflet movements as an indicator of crop water stress 1. Crop Sci. 25 (6), 1101–1106. http://dx.doi.org/10.2135/cropsci1985.0011183X002500060048x.
Pastenes, C., 2004. Leaf movements and photoinhibition in relation to water stress in field-grown beans. J. Exp. Bot. 56 (411), 425–433. http://dx.doi.org/10.1093/jxb/eri061.
Sakowska, K., Alberti, G., Genesio, L., Peressotti, A., Delle Vedove, G., Gianelle, D., Colombo, R., Rodeghiero, M., Panigada, C., Juszczak, R., et al., 2018. Leaf and canopy photosynthesis of a chlorophyll deficient soybean mutant. Plant Cell Environ. 41 (6), 1427–1437. http://dx.doi.org/10.1111/pce.13180.
Verger, A., Vigneau, N., Chéron, C., Gilliot, J.-M., Comar, A., Baret, F., 2014. Green area index from an unmanned aerial system over wheat and rapeseed crops. Remote Sens. Environ. 152, 654–664. http://dx.doi.org/10.1016/j.rse.2014.06.006.
Verhoef, W., 1984. Light scattering by leaf layers with application to canopy reflectance modeling: The SAIL model. Remote Sens. Environ. 16 (2), 125–141. http://dx.doi.org/10.1016/0034-4257(84)90057-9.
Vincent, R.K., 1972. An ERTS Multispectral Scanner Experiment for Mapping Iron Compounds. Technical Report.
Woebbecke, D.M., Meyer, G.E., Von Bargen, K., Mortensen, D.A., 1995. Color indices for weed identification under various soil, residue, and lighting conditions. Trans. ASAE 38 (1), 259–269. http://dx.doi.org/10.13031/2013.27838.
Yang, X., Li, R., Jablonski, A., Stovall, A., Kim, J., Yi, K., Ma, Y., Beverly, D., Phillips, R., Novick, K., et al., 2023. Leaf angle as a leaf and canopy trait: Rejuvenating its role in ecology with new technology. Ecol. Lett. http://dx.doi.org/10.1111/ele.14215.
Yang, G., Liu, J., Zhao, C., Li, Z., Huang, Y., Yu, H., Xu, B., Yang, X., Zhu, D., Zhang, X., et al., 2017. Unmanned aerial vehicle remote sensing for field-based crop phenotyping: current status and perspectives. Front. Plant Sci. 8, 1111. http://dx.doi.org/10.3389/fpls.2017.01111.
Zhou, Q.-Y., Park, J., Koltun, V., 2018. Open3D: A modern library for 3D data processing. arXiv:1801.09847.
Zink, M., Samaniego, L., Kumar, R., Thober, S., Mai, J., Schäfer, D., Marx, A., 2016. The German drought monitor. Environ. Res. Lett. 11 (7), 074002. http://dx.doi.org/10.1088/1748-9326/11/7/074002.
Zou, X., Mõttus, M., 2015. Retrieving crop leaf tilt angle from imaging spectroscopy data. Agricult. Forest. Meterol. 205, 73–82. http://dx.doi.org/10.1016/j.agrformet.2015.02.016.
Zou, X., Mõttus, M., Tammeorg, P., Torres, C.L., Takala, T., Pisek, J., Mäkelä, P., Stoddard, F., Pellikka, P., 2014. Photographic measurement of leaf angles in field crops. Agricult. Forest. Meterol. 184, 137–146. http://dx.doi.org/10.1016/j.agrformet.2013.09.010.